ABSTRACT

Title of Thesis: RAPID POLYMER PROTOTYPING FOR LOW COST AND ROBUST MICROROBOTS

Jessica Rajkowski, Master of Science, 2010

Research directed by: Professor Sarah Bergbreiter
Department of Mechanical Engineering
and The Institute for Systems Research

The Rapid Microrobot Prototyping (RaMP) Process uses Loctite® photo-patternable polymer products and photolithography to rapidly fabricate robust, inexpensive, and compliant robots. The process is developed and examined on two size scales. On the size scale of several centimeters, two functional robots and a small gripper have been designed and demonstrated with shape memory alloy (SMA) used for actuation. The gripper is 1.2 g and costs $3.21 while the inchworm robot is 7.4 g and costs $7.76 in small numbers. The second robot costs $14.93 in small numbers. On the sub-centimeter scale, designs and considerations for a walking microrobot fabricated with the process and its control are fully described. The design and kinematics of a thermally actuated, one degree of freedom leg for the microrobot are developed and simulated. Several of these units could be combined to rapidly build a 30 mg functional and simple walking microrobot with the ability to lift several grams.

RAPID POLYMER PROTOTYPING FOR LOW COST AND ROBUST MICROROBOTS

by

JESSICA ELIZABETH RAJKOWSKI

Thesis submitted to the Faculty of the Graduate School of the

University of Maryland, College Park in partial fulfillment

of the requirements for the degree of

Master of Science

2010

Advisory Committee:

Professor Sarah Bergbreiter, Chair/Advisor

Professor Don DeVoe

Professor Elisabeth Smela

Acknowledgements

There are many people who deserve thanks for their assistance and contributions to this thesis. I would like to thank the members of the Microrobotics Lab for their advice and time throughout this project. I would especially like to thank Aaron Gerratt for his help with the simulations and for his constant contribution of ideas. I also would like to thank Dave Bonanno for his help on putting together the control circuit for the little hexapods.

I would like to thank Dr. Elizabeth Smela and Mario Urdaneta at the University of Maryland for their advice and assistance throughout this project. Much of the work in this thesis was inspired by their research on Benchtop Polymer MEMS. I would also like to thank Bavani Balakrisnan for her collaboration with me on the thermal actuators.

Mostly, I would like to thank my graduate advisor, Dr. Sarah Bergbreiter, for her guidance and patience, not only regarding research, but with life in general.

I also gratefully acknowledge the support of NSF for the funding of this project.

Table of Contents

List of Tables

List of Figures

Chapter 1

Introduction

Interest in fabricating large numbers of small robots has grown recently due to applications ranging from mobile sensor networks to search and rescue. However, realizing these applications is difficult due to the extended fabrication time, cost, and fragility of current robot manufacture and design. The RaMP Process presented in this work was developed to quickly fabricate large numbers of inexpensive, robust and compliant robots, both on the centimeter and millimeter scales. Milli-robots are defined as centimeter-sized robots with millimeter-scale features. Likewise, microrobots are defined as millimeter-sized robots with micron-scale features.

1.1 Cost

In developing the process, one of the most important goals was keeping the cost of fabrication down. The high cost of fabrication on this scale is one of the main factors hindering the progress and feasibility of these robots. It was important that this process be able to keep the per-robot cost down to only a few dollars and limit the start-up costs. This can be achieved by using inexpensive materials that can be used outside of cleanroom facilities and without the expensive silicon processing equipment that drives up the cost of microrobots [1]. In addition, the process should be made compatible with batch fabrication so that the costs can be divided over

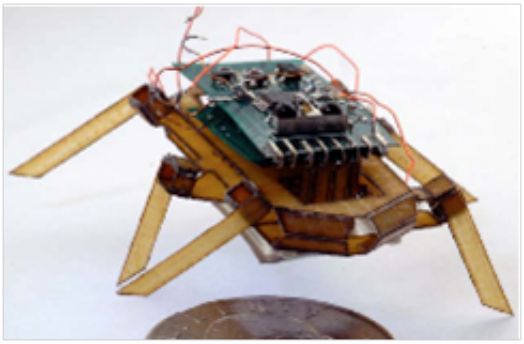

Figure 1.1: The RoACH Robot made using Smart Composite Microstructures [3]

several robots.

Several mobile robots have been demonstrated at the centimeter-scale [2, 3] but they cannot currently be manufactured in large numbers and have high one-time equipment costs, including laser cutting machines that cost in the tens of thousands of dollars (Figure 1.1). These robots can also require long assembly times, costing even more money.

1.2 Design and Fabrication Time

In addition to cost, long fabrication times severely limit the feasibility and practicality of tiny robots. Design iterations can take months, which makes progress in this area unnecessarily slow [4]. The use of polymers will allow many milli-robots to be fabricated in less than an hour on a benchtop and microrobots to be fabricated in less than a day instead of several weeks in a cleanroom or after many hours of assembly. Although this process will not be able to replace the traditional MEMS devices, due to resolution limitations, it could be used as a platform to test ideas for these smaller microrobots, potentially saving months of time in design and testing

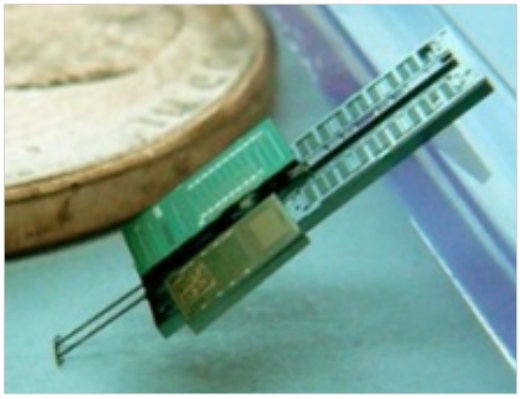

Figure 1.2: Jumping MEMS Robot by Sarah Bergbreiter [4]

cycles.

1.3 Robustness

This new process also targets improved robustness through the use of polymers and compliant mechanisms. Microrobots demonstrated to date [5, 6] suffer from fragile mechanisms as a result of traditional MEMS processing materials and techniques (Figure 1.2). Low Young's modulus polymers will add compliance to otherwise fragile robots. Polymers can also be used to embed other robot components such as actuators and wiring, which eliminates the danger of damage and having these components fail due to contamination (Figure 1.3). Similar ideas have been demonstrated successfully in larger robots using shape deposition manufacturing [7], but have yet to be demonstrated in small-scale robots (Figure 1.4). Successful robots on the centimeter scale have yet to demonstrate robust integration [2, 3].

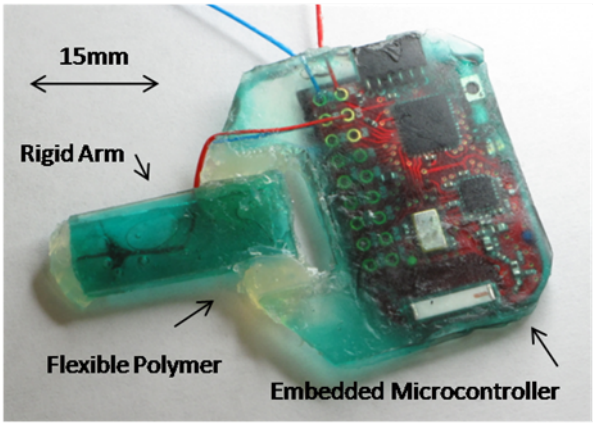

Figure 1.3: Mockup of an inchworm robot with embedded radio and microcontroller (TI EZ430-RF2500) to wirelessly monitor and control the robot. The green layer is a rigid polymer while the clear is more elastic.

Figure 1.4: Robotic leg fabricated with Shape Deposition Manufacturing [7]

1.4 Functionality

In addition to fabrication difficulty, cost, and fragility, another challenge for small robots is moving through unpredictable environments [8]. As the robots grow smaller, obstacles around them grow proportionally larger with respect to the robot size. Combining polymers with varying material properties allows for creation of complaint mechanisms that have proven successful in overcoming obstacles and unpredictable environments at large scales [9, 10]. However, little has been done to demonstrate this in small-scale robots.

The process outlined in this work uses compliant photo-patternable materials to combine the benefits of small-scale robots with the robustness and compliance in larger-scale robots. Compliant mechanisms will improve the mobility and robustness of robots on the centimeter and millimeter-scales and can also be used to add mechanical energy storage for improved efficiency. While this process is currently limited to planar structures, separately constructed components can be stacked and folded to create more complex robots. Also, the addition of a folding step allows for three-dimensional structures to be realized.

1.5 Actuation

Another challenge to demonstrating a successful microrobot fabrication process is integrating actuation. Thermal actuators have been extensively used in microrobotics and MEMS devices [11, 12, 13]. This is mainly due to their simplicity, robustness and high force outputs, making them ideal for proof-of-concept and pro-

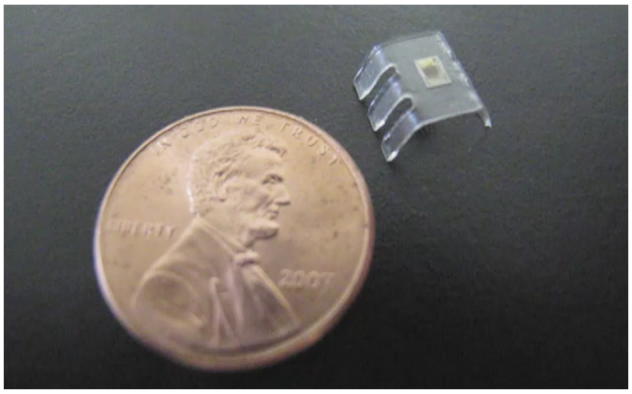

Figure 1.5: Loctite®3525 photpatternable acrylic hexapod microrobotic platform with embedded microprocessor.

totyping. Although they require high power, they remain attractive due to their ease of fabrication and integration with MEMS devices. While more efficient actuators will eventually be explored for integration, the use of thermal actuators will allow quick development and testing of many functional and robust robots. This will be essential to the design and fabrication of mobile robots at the sub-cm scale.

This work has approached these goals on two size scales. In Chapter II, the Rapid Microrobot Prototyping (RaMP) Process and considerations are presented. Then, demonstrations of using RaMP to fabricate functional milli-robots are given. In Chapter III, it is shown how some slight modifications to the process add additional functionality for making smaller and more efficient robots. After shrinking the process down, we present the design, simulation and testing of a thermally actuated leg component as well as considerations for the design of a polymer microrobot, a mock up of which can be seen in Figure 1.5. Procedures used to scale down the process, including thermal actuators on a polymer platform, are presented and microrobot results, calculations and demonstrations are discussed. In Chapter

IV, additional applications of the process that were not previously discussed are presented.

Chapter 2

Rapid Microrobot Prototyping Process

The goal of this initial research was to develop a fabrication process that is fast, inexpensive, and allows for the creation of many functional and robust robots that can be made at the centimeter and eventually the millimeter-scale, as well as testing designs for smaller robots. In Section 2.1, the procedures used to create multi-material compliant robot flexures using the RaMP process are presented. In Section 2.2, process characterization including achievable feature resolution is discussed. In Section 2.3, integration of actuation into the process is described, and Section 2.4 details the design, fabrication and testing of an inchworm robot and a robotic gripper. Finally, in Section 2.5, it is shown how a modification can be made to the original process to increase functionality to allow the fabrication of multi-layered robots.

2.1 Fabrication Process

In order to keep this process quick and inexpensive, it should take place outside of a cleanroom, without expensive equipment, and all materials need to be easy to work with. For eventual use with millimeter-scale robots, the process should also be scalable to smaller sizes. Finally, batch fabrication techniques will allow for large numbers of robots to be fabricated at once. All of these requirements were

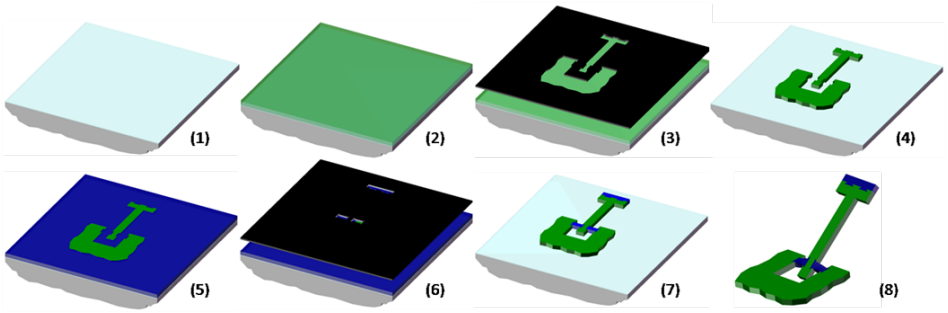

Figure 2.1: The Rapid Microrobot Prototyping (RaMP) Process. The different color components represent materials with different Young's Moduli - green represents a more rigid polymer and the blue is a soft, flexible silicone.

considered in developing the process.

Loctite® photo-patternable adhesives and silicones are available with a range of material properties. This work will focus on Loctite® 3525, an adhesive, and Loctite® 5084, a silicone product. Loctite® 3525 is a modified acrylic and was chosen for its stiffness and moderate modulus of 175 MPa [14]. Loctite® 5084 is an alkoxy silicone that has high strength and is extremely flexible [15]. These products do not have adverse health effects, so no additional protection or equipment is necessary. Choosing materials of drastically different Young's moduli allows for investigation of robotic flexures made from both rigid and compliant parts. These materials have not been used before to create multi-material mechanical components, although Loctite®photo-patternable adhesives have been used to create microfluidic devices [16].

2.1.1 *Process*

The process flow is described in Figure 2.1. In step 1, uncured Sylgard® 184 silicone elastomer base (without the curing agent) is spread evenly in a thin layer over the substrate. This ensures easy release of the structure after patterning is complete. This step can be avoided if using a non-stick substrate such as a surface with cured poly dimethylsiloxane (PDMS) silicone. The first polymer to be patterned is then applied in step 2. Desired thickness of the polymer is achieved by the use of spacers of known thickness such as glass slides or coverslips. For the purpose of this research, thicknesses of 180, 350 and 1100 μms were used. A given thickness can also be achieved by spin coating on a flat substrate. The exact final thickness of the cured polymer can be determined using a profilometer or calipers for thicker samples.

After the first polymer is deposited at its desired thickness, it is patterned using an inexpensive transparency mask in step 3. The polymers used for this demonstration were negative resists so all masks were dark field. The masks used were also coated with a thin layer of Sylgard® 184 elastomer base to prevent the polymer from bonding to it. The polymer is then cured directly under the light from a portable UV lamp (Spectroline®, EN-180, 365 nm). Cure times for the polymers at each thickness are displayed in Table 2.1 and are generally a couple minutes long, depending on layer thickness.

After curing, the mask is removed. Uncured polymer is washed away mechanically with water, followed by a solvent such as acetone. After this, the polymer is given a final rinse with water to remove any re-deposited polymer and excess

Table 2.1: CURE TIMES FOR POLYMERS (MIN:SEC)

Thickness (μm)	Loctite® 3525	Loctite® 5084
180	0:50	2:20
350	1:40	4:70
1100	7:30	8:00

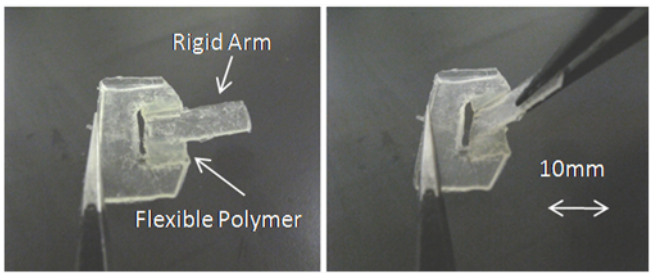

Figure 2.2: A 0.3 g bi-material torsion hinge produced with the RaMP Process.

acetone in step 4. In step 5, the second polymer is applied. It is flattened to the desired height using spacers or the height of the first cured polymer. This second polymer is patterned with its respective mask in step 6, and cured and rinsed using the same technique as noted previously in step 7. More polymers can be patterned in subsequent steps. Finally in step 8, the entire structure is peeled from the substrate with the resulting fabricated structure shown in Figure 2.2. All parts of this process were carried out under normal lighting conditions and can be done outside of a cleanroom environment.

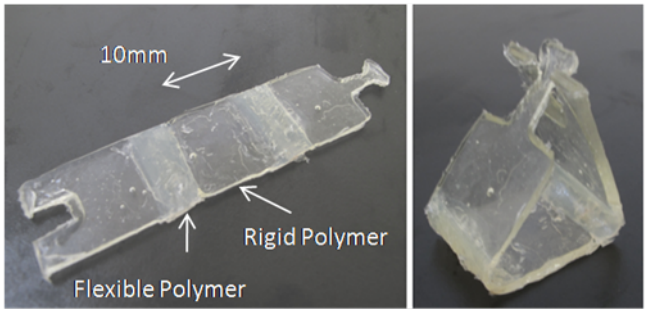

Figure 2.3: Planar bi-material features can be fabricated, folded, and secured out-of-plane to build 3-D structures.

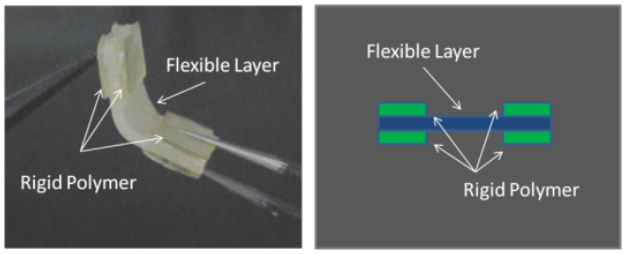

Figure 2.4: Layers can be fabricated on top of each other or stacked to form complex 3-D structures.

2.1.2 *3-D Structures*

Although this fabrication method is a planar process, it can be used to make mechanisms that are not limited to planar structures. Layers can be stacked or folded to create three dimensional structures similar to those in [2, 17] as seen in Figures 2.3 and 2.4. However, this added design complexity and the required folding to achieve these 3-D structures limits the ability to batch fabricate components.

2.1.3 *Process Considerations*

Several additional process steps can be used to add to the basic functionality described in the RaMP Process. For example, embedding components needs to take

place before the polymer is cured. The components, e.g. the controller or actuators, can be placed in the uncured polymer, pushed down or covered with additional polymer and the process can continue as described above. In addition, a diluting material can be added to create thinner layers with viscous polymers. This has been demonstrated with silicone using n-heptane to dilute and spin-coat a material that otherwise would not be capable of producing consistent layers [18]. During the curing process, the polymers must be covered to protect from oxygen exposure. In the process previously described, the mask served as an oxygen barrier, however if contact lithography is not used, it is necessary to cover the polymer separately or create a nitrogen environment. Without this, the polymer will react with the oxygen during crosslinking and leave a layer of uncured polymer [16].

The cured polymer, particularly in thicker samples, will often get small bubbles of trapped air. These have not seemed to affect the functionality of our components; however, at a smaller scale it is feasible that they may become a more significant problem. This can easily be managed by placing the setup in a vacuum to pull the bubbles out. It is also important to note that the cured polymer will appear cloudy even in the absence of such bubbles and regardless of the cleaning process.

Determining the order in which polymers are applied can also be important. The first polymer to be applied is typically the one with better feature resolution, although reversal of this order is possible and will still yield results. However, smaller features and improved designs were seen by defining the smallest features first.

Finally, the device will release from the substrate more easily when it is allowed to cure for a bit longer in ambient air and light after all excess polymer has been

removed. A few hours will allow it to completely finish curing and the result can be easier to work with. However, this step is not necessary and similar results are obtained without taking this extra time.

2.2 Process Characterization

To support usability and scalability in the RaMP Process, bond strength between polymers and feature size resolution are both characterized. Initial characterization by manually pulling apart two attached polymers has demonstrated strong adhesive bonds between Loctite® 3525 and 5084 by simply curing the polymers in contact with each other. However, this result does not occur with all Loctite® photo-patternable adhesives. For example, Loctite® 3108 does not adhere well to 5084. Bonding can be enhanced by use of structures to increase bond surface area when using products that do not bond well together or when there is only a limited surface area for bonding. Finger-like protrusions and other mechanical shapes have been demonstrated to increase surface area and bonding between polymers (Figure 2.5). Future research is still needed to test the strength of the bonds and their durability over spans of time and number of uses.

Minimum feature sizes are shown in Table 2.2 and Table 2.3 and were measured using the resolution test in Figure 2.6. For the purpose of this research, resolution was defined as the smallest feature that could be resolved without growth surpassing ten percent of the intended feature size. Growth is defined as fabricated feature expansion beyond the feature drawn on the mask. These tests were carried out using

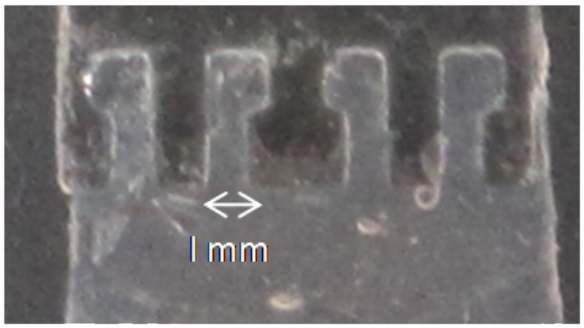

Figure 2.5: Adhesion enhancement structures.

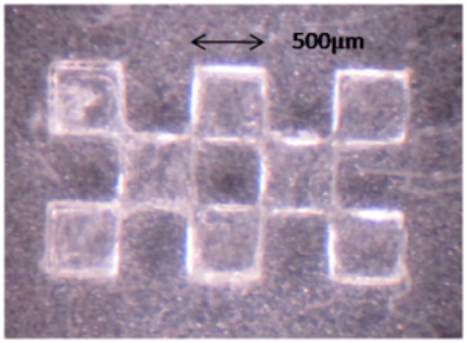

Figure 2.6: Resolution test of 180 μm thick Loctite® 3525. Feature sizes are 500 μm.

Table 2.2: RESOLUTION WITH COMMERCIAL MASK

Thickness (μm)	Loctite® 3525	Loctite® 5084
180	250 μm	1250 μm
350	500 μm	1250 μm
1100	2000 μm	3750 μm

Table 2.3: RESOLUTION WITH INK-JET MASK

Thickness (μm)	Loctite® 3525	Loctite® 5084
180	750 μm	2000 μm
350	1000 μm	3000 μm
1100	2000 μm	20 mm

commercially purchased laser printed masks (∼$25/mask) as well as extremely inexpensive masks made with an ink-jet printer (Canon Pixma iP4500, 9600x2400 dpi) on inkjet film (AccuBlack® from Chromaline®). At less than a dollar per sheet, and immediate turnaround, the process time and cost is further reduced by printing the mask instead of out-sourcing it. However, one drawback of inkjet printing is lower resolution.

As seen in Tables 2.2 and 2.3, feature sizes increase with increased thickness regardless of the mask type. There is significantly more growth when a thicker

layer of polymer is used, so the minimum feature size becomes much larger. Minimum feature sizes achieved with Loctite® 5084 are larger than those achieved with Loctite® 3525. Loctite® 5084 also becomes very weak in regards to the structural integrity of the material at thicknesses less than 300 μm. As a result, it is difficult to achieve freestanding and defined features at this size with Loctite® 5084. To solve this problem, a stronger polymer should be used at these thicknesses. In addition, smaller feature sizes do not retain full layer thickness. This is likely due to exposure intensity and polymer chemistry, although further testing is needed to determine exact cause.

2.3 Integrating Actuation

Once compliant mechanisms have been designed, the next step is to integrate actuators with the prototyping process. Shape memory alloy (SMA) wires were chosen for the robot actuators (Flexinol® Nitinol 0.0100" dia) due to their simplicity and robustness. SMA has also been processed and demonstrated at the micro-scale, although only macro-scale SMA is used in this work. [19, 13, 12]. These metal wires have the ability to "remember" a predetermined shape and return to it when heated. The popularity of using SMA as an actuator is growing due to its several advantages including high-power to weight ratio and the large deformation capacity.

Shape memory alloys are also relatively easy to work with. For actuation of robot flexures, large displacements were required. For this reason, SMA was trained into tightly wound coils. The untrained SMA was wrapped around a metal rod

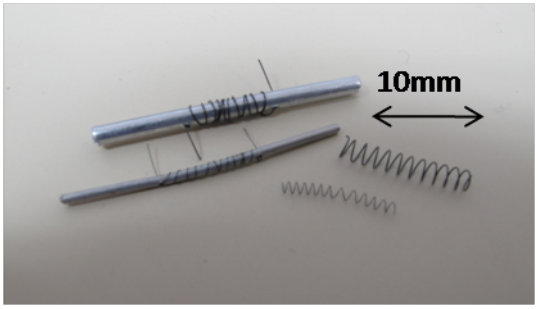

Figure 2.7: Setup for training shape memory alloy (SMA) into tightly wound coils for robot actuation. Heating after deformation will return the springs to their trained position.

of desired diameter (Figure 2.7) and placed on a pre-heated hot plate at 540 °C (Fisher Scientific Isotemp Ceramic120 V, 60 Hz). The SMA was then removed after 20 minutes, at which point it was quenched in water to ensure swift cooling. This step is necessary to avoid brittleness in the SMA. After removing the SMA from the metal rod, it is ready to be integrated into the polymer robot.

Once trained, it is important not to over stretch the actuator because this will deform the SMA plastically and it will not retain its shape memory. It is also important that the SMA is not heated much higher than the activation temperature. This will result in the SMA working poorly or failing to work at all. In addition, it has been shown that the coils, if left in tension for long periods of time on the order of several weeks, will also lose some memory and not fully return to the trained form when heated.

After the SMA is trained and cut to the desired shape and size, metal clips are attached to the ends. Wires cannot be directly soldered to the SMA using traditional solder, so the wires are instead soldered to these clips. The ends of the SMA can then be embedded into the polymer during fabrication and the polymer

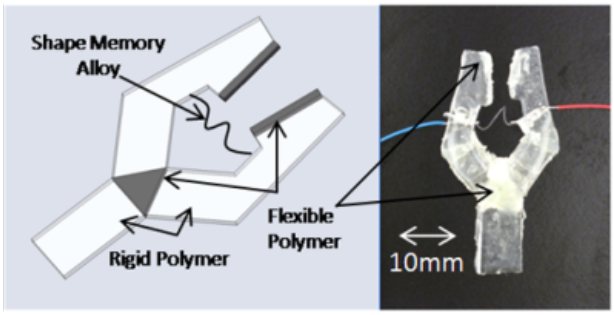

Figure 2.8: Gripper made using the multi-material prototyping process.

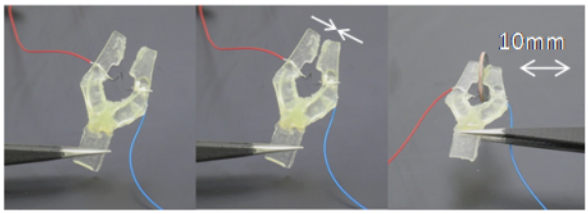

Figure 2.9: Frame shots of gripper actuation. In the last frame, the gripper holds a dime.

is cured with the SMA in position.

SMA is a high power actuator. However, it is also inefficient and therefore unacceptable for the final goal of building autonomous robots. For this reason, these actuators will be eventually be replaced with low-power actuators such as electrostatic inchworms, PZT, or dielectric elastomer actuators (DEAs) [20, 21]. The advantage of DEAs is that these could eventually be batch fabricated with the mechanisms since similar compliant polymers are required.

2.4 Robot Design and Results

2.4.1 *Gripper Arm Design*

Using the process described above, a one degree-of-freedom gripper arm was fabricated using a single piece of shape memory alloy for actuation. The Solidworks® design is shown juxtaposed with the fabricated device in Figure 2.8. This gripper uses the softer Loctite® 5084 as a compliant joint between the two gripping fingers as well and also provides a softer material on the fingers. This added compliance allows the gripper to grip objects of varying sizes and shapes [6]. The more rigid Loctite® 3525 serves as the gripper skeleton and a single piece of SMA is used to pull the fingers together. This fabricated gripper is approximately 40 mm long, 20 mm wide, and 1 mm thick, and weighs 1.2 grams. In Figure 2.9, frame shots are shown of the gripper actuating and grasping a dime. A United States Dime weighs approximately 2.27 grams. The diameter is 17.9mm with a thickness of 1.4 mm. This gripper was put through testing to determine its long term durability. After over 5000 cycles and three days, the gripper continued to actuate.

2.4.2 *Inchworm Robot Design*

To further illustrate the capability of this process to fabricate mobile robots, we have fabricated a tethered, one degree-of-freedom crawling robot as seen in Figure 2.10. The polymers were strategically placed to provide the friction characteristics needed for the robot to move forward in an inchworm-like gait. The soft Loctite® 5084 is placed on the end of the robot to anchor the back of the robot

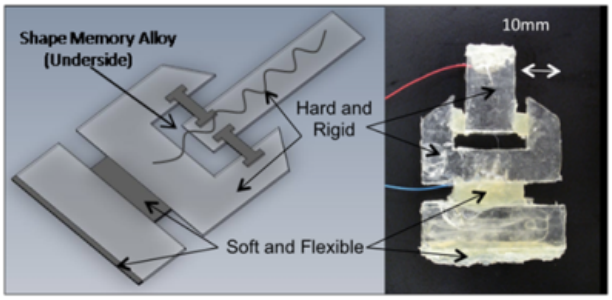

Figure 2.10: Design of a 7.4 g inchworm robot with a 1.2 cm step size.

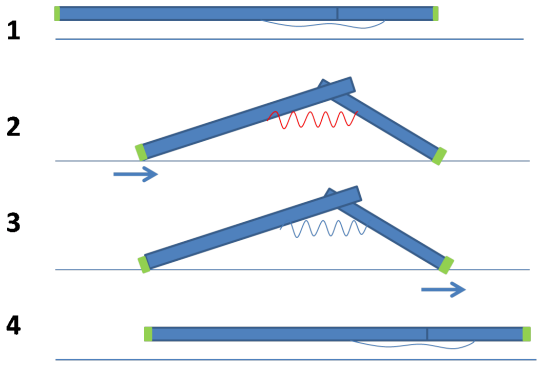

Figure 2.11: Illustration of the Inchworm Gait. In step one, the SMA is unactuated. In step two, the SMA is actuated, and the back of the robot is pulled forward. In step three, the SMA is unactuated and the front of the robot slides forward until it is relaxed in step four.

when the leg is released. A separate stacked layer of Loctite® 3525 on the back of the robot allows the robot rear to slide forward when the leg is actuated. This crawling motion from directional friction is possible due to the varying coefficients of friction of the two polymers used. An illustration of this gait is shown in Figure 2.11.

The current inchworm robot uses a single SMA wire for actuation, and frame shots of the robot crawling can be seen in Figure 2.12. The final prototype is less than 7 cm long, 4.5 cm wide, 2 mm thick and weighs 7.4 grams. The robot step size is measured at 1.2 cm. The cycle time per-step on this robot is about six seconds,

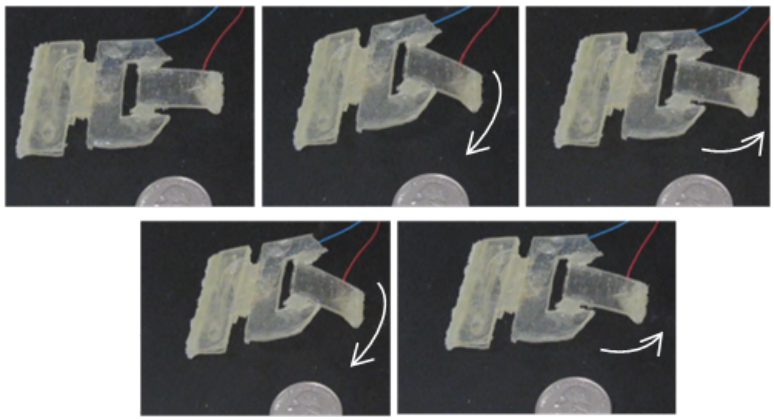

Figure 2.12: Frame shots of an inchworm robot walking forward. A quarter is placed for scale.

however, this can be sped up significantly. Firstly, this robot was controlled by manually adjusting the current. If control were developed that would oscillate the temperature right around the transition temperature of the SMA, it would not be over-heated and therefore would take less time to cool. Also, if made smaller, the inchworm robot would require less force and could be actuated with a thinner wire. This thinner wire would cool much faster then the current wire thickness. Both of these improvements would also decrease the power consumption of the robot. While it currently requires 1W to actuate the SMA, using optimized control or smaller wire would decrease this significantly. Past research as concluded that Nitinol wire with thickness on the order of 30 μm that is heated just above its transition temperature, will have a cooling or relaxation time of about 0.2 seconds [22].

While this robot only demonstrates a single degree of freedom leg, the process can easily be extended to fabricate more complex multi-degree of freedom robots. Both the gripper and the inchworm robot have easily survived multiple several-foot drops.

Figure 2.13: MEMS gears fabricated with sacrificial layers. Picture courtesy of Sandia National Laboratory, SUMMiT (TM) Technologies, `www.mems.sandia.gov`

2.5 Extension of Process to Many Layers

The process described in the previous sections limits the design capabilities to stacked layers or planar structures. Although folding is another possibility with the process, a sacrificial layer must be integrated in order for it to generate more complex 2.5-D mechanisms like bridges or other overlapping, non-connected structures (Figure 2.13). This is necessary for it to be competitive with other processes available at the centimeter scale. The design capabilities of the process are severely limited without a sacrificial layer.

For this application, a sacrificial layer was needed that could be used on a benchtop without the use of harsh chemicals. Also, it needed to have the ability to be poured over the existing polymer structures so that they could be planarized and be made rigid enough to build on top of. In addition, it needed to be a material that

could be removed without damaging the polymer structures of the robot. Several sacrificial materials were investigated and tested, including Cyclododecane wax. This wax could be heated to liquid form and poured. It solidified quickly, and was easy to build upon. The wax could be removed by heating at a low temperature. However, after removal, the polymer was left with a waxy coating. As a result, other options were explored.

It was shown that gelatin could be used with relative ease and accuracy. It too could be poured and solidified quickly. It was easily removed with warm water and left little or no residue. The gelatin used was Knox ®original unflavored gelatin. The powder is mixed with hot water and left on a hot plate to maintain temperature during processing. It is important to use unflavored gelatin because the additional ingredients included in flavored varieties significantly increase the time needed to solidify, which will in turn, significantly increase fabrication time. It may be useful to color the dye to help distinguish it from the surrounding polymer. To facilitate this, food dye or coloring can be added with no detrimental effects on the process.

2.5.1 *Process*

The process for fabrication with a sacrificial layer only requires a slight modification to the RaMP process described previously. The new process flow is described in Figure 2.14. Step 1 is the same as in the original process, except for that it must be done inside a portable container with a lip to constrain the sacrificial layer, such as a petri dish. Step 2 can be achieved with the RaMP process as described earlier

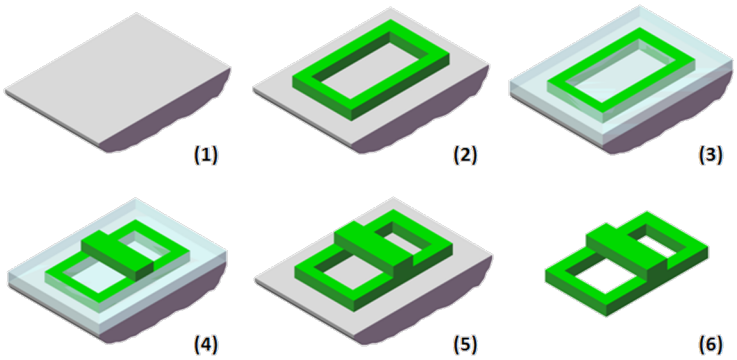

Figure 2.14: The RaMP process for many layers. The green material is the Loctite® polymer and the blue transparent material is the sacrificial layer.

in Section 2.1.1. In step 3, the surface is planarized with gelatin and put into a refrigerator to be solidified. Within ten minutes, the gelatin is solid and can be built on top of. In step 4, the RaMP process is repeated on this newly planar surface. This can be repeated until as many layers as needed in the design are created. In step 5, the gelatin is removed with warm water, and the multi-layer structure is removed from the substrate in step 6.

To get the best results with this modified process, care must be taken to keep the gelatin from getting warm during the UV exposure. This was solved by conducting the process on top of a cold metal platform. The petri dish was simply placed on top of a piece of metal that we kept in the freezer when not in use. This kept the gelatin cold enough to remain sold thoughout the curing time for the polymer.

2.5.2 *Multi-layer Robot Results*

A walking multi-layer polymer robot was designed and fabricated using this process. As seen in Figure 2.15, the robot had four one degree of freedom legs and two actuators. Once again, shape memory alloy was integrated with the processed mechanisms to provide the actuation necessary. A computer model of the robot is included to more clearly show the design (Figure 2.16). The robot walked by first lifting two legs oriented in the same direction, using shape memory alloy. This moves the robot forward one step length. Then the other actuator is engaged, moving the other set of legs to the ground. At this point, the first set of legs is disengaged followed by the second. When the second set of legs disengages, the robot is again moved forward one step length. This control sequence is repeated for continuous walking. This gait is illustrated in Figure 2.17

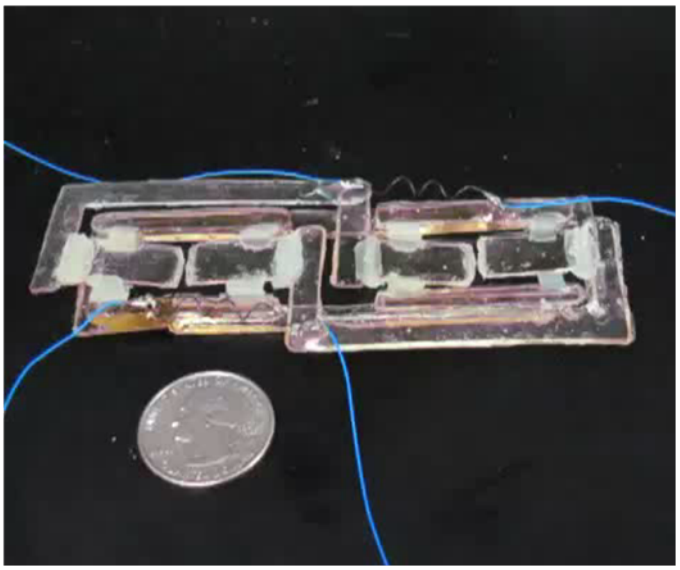

Figure 2.15: A four legged robot fabricated using the polymer process with a sacrificial layer. A quarter is placed for scale.

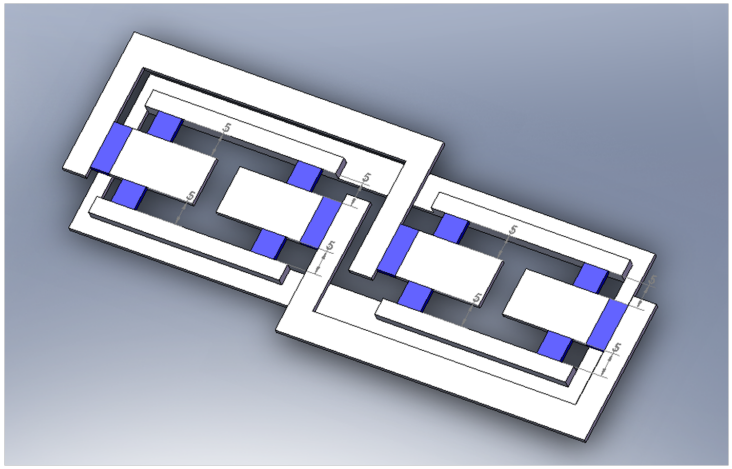

Figure 2.16: The design of the four legged robot.

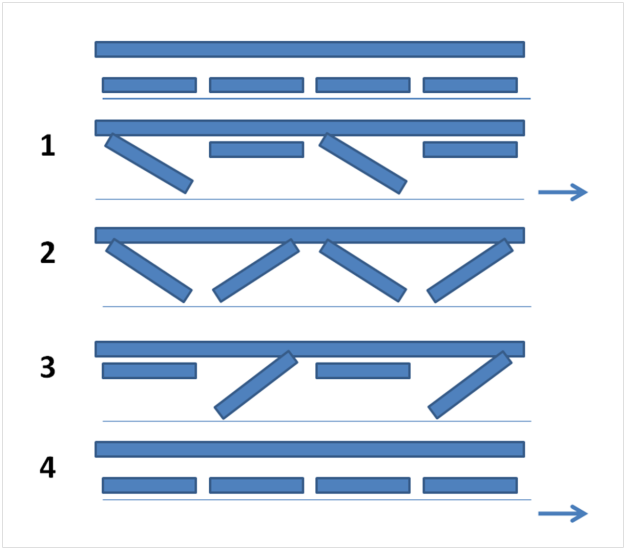

Figure 2.17: The gait of the four legged robot. The robot makes forward motion in steps one and four.

The power required and step size is similar to that of the inchworm robot. Each actuator draws approximately 1 W of power. This is very high power, but this robot walks much more consistently and has the ability to carry higher loads than the inchworm robot because it is not dependent on differential friction between the front and the back. The robot suffers from the same slow actuation times as the inchworm due to the extended time for the SMA to cool down by air convection, but as mentioned earlier with respect to the first robot, this would also be sped up by making the robot, and thus actuators, smaller or using more accurate and optimized control.

2.6 Robot Cost Analysis

A primary motivation for this research is to find a cost and time effective alternative to the expensive traditional methods of prototyping small-scale robotics. For this process, there are several one-time costs as well as per-device costs, as seen in Tables 2.4, 2.5, and 2.6. These costs include a printer for mask production, a UV lamp for curing polymers, and a hot plate for training of SMAs. Per-device costs include the polymers, transparencies for mask production, and SMA for actuation. The majority of the per-device cost is the polymer materials. These costs can all be reduced by buying in large, bulk quantities. Costs can also be reduced by recycling the masks.

The second advantage of this process is that it allows for prototyping of many designs quickly. Designs can be designed, fabricated, analyzed, and re-designed in

Table 2.4: COST ANALYSIS-ONE TIME COSTS

Product	Cost
Ink-Jet Printer (Canon PIXMA iP4500)	$119.99
UV Lamp (Spectroline EN-180 365 nm)	$157.77
Hot Plate (Fisher Scientific Isotemp Ceramic 120 V)	$232.87
Glass Microscope Slides (Quantity:72)	$49.40
Sylgard 184, 0.5 kg	$51.86
Acetone, 4 L	$98.40
	Total $710.29

Table 2.5: COST ANALYSIS-PER GRIPPER COSTS

Product	Cost
Mask Film (assuming ink-jet printed)-one sheet	$0.96
Transparency Substrate-one sheet	$0.60
Shape Memory Alloy (0.01" dia-$35/25 ft)-approx 1 inch	$0.14
Loctite® 3525 ($28/25 ml syringe)-1 ml	$1.40
Loctite® 5084 ($68.75/10.8 fluid ounces)-0.5 ml	$0.11
	Total $3.21

Table 2.6: COST ANALYSIS-PER INCHWORM ROBOT COSTS

Product	Cost
Mask Film (assuming ink-jet printed)-one sheet	\$0.96
Transparency Substrate-one sheet	\$0.60
Shape Memory Alloy (0.01" dia-\$35/25 ft)-approx 2 inch	\$0.28
Loctite® 3525 (\$28/25 ml syringe)-4 ml	\$5.60
Loctite® 5084 (\$68.75/10.8 fluid ounces)-1.5 ml	\$0.32
	Total \$7.76

Table 2.7: COST ANALYSIS-PER WALKING ROBOT COSTS

Product	Cost
Mask Film (assuming ink-jet printed)-one sheet	\$0.96
Transparency Substrate-one sheet	\$0.60
Shape Memory Alloy (0.01" dia-\$35/25 ft)-approx 4 inch	\$0.56
Loctite® 3525 (\$28/25 ml syringe)-8 ml	\$11.20
Loctite® 5084 (\$68.75/10.8 fluid ounces)-6 ml	\$1.28
Unflavored Gelatine (\$1.32/1 ounce)-0.25 ounces	\$0.33
	Total \$14.93

short periods of time. Moving from a robot design to a fabricated and functional robot takes less than one hour in the case of the inchworm robot, or less than a few hours for the multiple layer robot.

2.7 Conclusions

Current small scale robots are expensive and require lengthy fabrication and assembly times. These robots also lack the compliance and robustness to perform well in unstructured environments. This chapter has described a new process to rapidly prototype inexpensive and robust centimeter-scale robots without the use of cleanroom facilities or expensive equipment. The use of Loctite® photo-patternable polymers can create several possibilities in the field of small robotics by eliminating the expense, fragility and complexity of traditional small-scale robots.

Chapter 3

RaMP at the Microscale

3.1 Robot Concept

After demonstrating the RaMP Process to make centimeter-scale robots, the next step was to explore using the process to make much smaller robots. Feature sizes mentioned in Chapter II allow for significant reductions in the size of the robots made with this process. The targeted robot body dimensions for this smaller robot are 9.5mm by 4mm, with legs that are 2.5mm long and 1.7mm wide, meaning that it should fit within a cubic centimeter (Figure 3.1). Working at scales that are an order of magnitude smaller than the previous demonstrations required exploration of other thermal actuation techniques to reduce assembly requirements for actuator integration. As robots get smaller, assembly becomes much harder and reducing these steps is necessary.

This chapter describes how to shrink the robots by using a new type of actuator, a twisting thermal bimorph. This includes how to integrate thermal bimorph actuators into the process and how, using an alternating tripod gait, these actuators can produce a walking microrobot. In Section 3.2, the design of the thermal actuator is discussed. Section 3.3 introduces a new actuator design to enable forward motion in the microrobot along with simulations showing the twisting functionality required. In Section 3.4, the procedures used to fabricate the microrobots, including

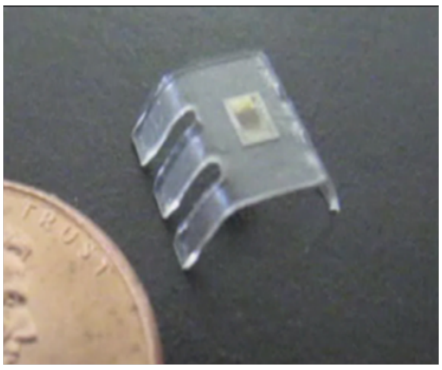

Figure 3.1: Targeted size of the microrobot. The robot body dimensions are 9.5mm by 4mm, with legs that are 2.5mm long and 1.7mm wide.

these thermal actuators on a polymer platform, are described. In Section 3.5, we discuss initial robot results and demonstrations, including integrating control and applying this new actuator to the design of a polymer microrobot.

3.2 Thermal Actuator Design

In order to successfully shrink the process down to eventually create a sub-centimeter crawling robot, a transition away from the shape memory alloy used with the larger robots needed to be made. Integrating the SMA at this scale would be significantly more difficult and time consuming. The new actuation technique needed to retain the simple fabrication of the larger robots, but at a much smaller scale. Although they require more equipment to fabricate, thermal bimorphs were chosen as actuators due to their simplicity, high force, and ease of integration at this scale. Thermal bimorphs are not a new concept. On the contrary, these thermal actuators are frequently used in MEMS. When a current is applied to a metal trace patterned onto a polymer, resistive heating causes both the copper and the polymer

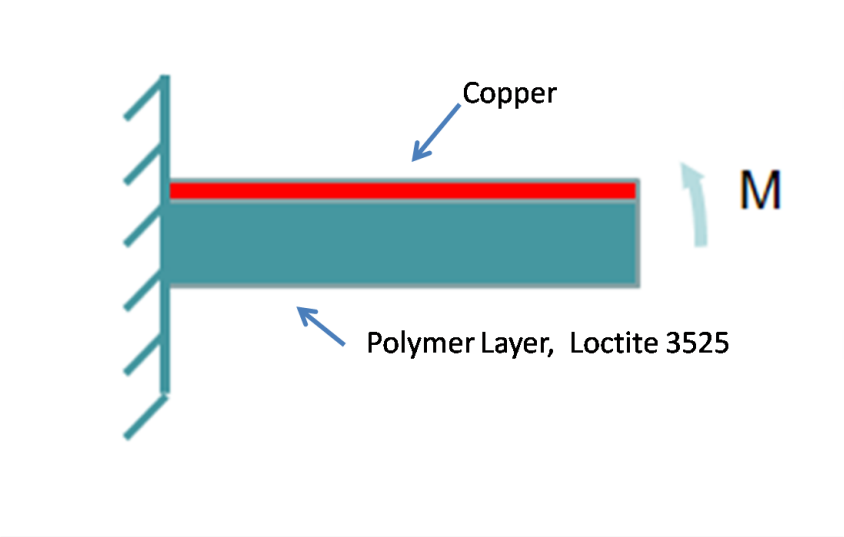

Figure 3.2: The concept of a bending thermal actuator. The top layer is copper and the bottom layer is Loctite® 3525. Copper has a much lower coefficient of thermal expansion then the polymer, causing the beam to bend upon heating.

to heat up and expand. Because the coefficient of thermal expansion of the polymer is larger than that of the copper, $(4.8 \times 10^{-4} K^{-1})$ and $(17 \times 10^{-6} K^{-1})$ respectively, the legs bend with the metal on the inside as seen in Figure 3.2 [14].

3.2.1 *Actuator Displacement*

Calculations for the expected bending were made using the Timoshenko Equation, shown here as Equation 3.1 [23]. Here, m is the ratio of the height of layer one to the height of layer two, h is the addition of the height of the two layers, or total leg thickness, and n is the ratio of the moduli. ΔT is the difference between the starting temperature and the final, elevated temperature, and the α terms are the respective coefficients of thermal expansion of the polymer and copper. In these calculations, ΔT is assumed to be 115 °C. This is assuming starting at room tem-

Table 3.1: CALCULATED DEFLECTION OF LEG WITH 1μm THICK COPPER

Polymer Thickness (μm)	Radius of Curvature (μm)	Deflection (μm)
300	4113	760
200	2666	1172
150	1971	1585
100	1297	2409

perature and hitting a maximum temperature of 140 °C. It was found in a separate experiment on a hot plate that at temperatures higher then 140 °C, the leg begins to suffer damage. The maximum deflection was taken right before the leg became damaged by the heat experienced. Finally, R is the radius of curvature of the leg. The results of these calculations for various polymer layer thicknesses are included in Table 3.1

$$\frac{1}{R} = \frac{(\alpha_1 - \alpha_2)\Delta T}{h} \frac{6(1+m)^2}{3(1+m)^2 + (1+mn)(m^2 + \frac{1}{mn})} \tag{3.1}$$

3.2.2 *Actuator Force*

$$\mathbf{F} = \frac{3EI_y}{2lR} \tag{3.2}$$

Force calculations were made to see how much weight this robot could carry using Equation 3.2, where EIy is the equivalent bending stiffness of the leg, l is the

Table 3.2: CALCULATED BLOCKED FORCE WITH 1μm THICK COPPER

Polymer Thickness (μm)	Blocked force (mN)
300	261.7
200	132.9
150	80.8
100	39.2

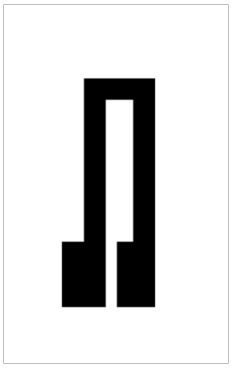

Figure 3.3: The design of simple bending actuators. This design is patterned on the legs that are used for lifting the microrobot.

length, and R is the radius of curvature [24]. The radius of curvature is taken from the previously discussed Timoshenko Equation. Considering a robot body and leg thickness of 150 μm, the expected blocked force from each straight leg is 80.0 mN. The expected blocked forces, or external forces required to keep the beam in plane, for the legs at different polymer thicknesses are displayed in Table 3.2. These also assume even temperature distribution and metal covering the entire surface, not just traces.

A close up of the copper pattern for the simple actuator design can be seen in Figure 3.3. The shape consists of a u-bend that goes over the leg and contact pads for applying the power.

3.3 Twisting Actuators

3.3.1 *Concept*

In order to reach our goal of demonstrating walking or forward motion of our microrobot with thermal bimorph actuators, an innovative gait or leg design is required. Walking with all actuators limited to the same 1-DOF has been demonstrated [5, 25], but this generally requires a unique leg orientation or complicated leg designs. We propose to approach this problem using twisting actuators on the legs to propel the body forward. By twisting, we mean one side of the leg deforming more than the other, resulting in a rotation of the leg around its length, and thus a force on the ground perpendicular to original the leg orientation and parallel to the ground.

$$\mathbf{R} = \frac{\rho * L}{A} \tag{3.3}$$

In order for this to work, a higher temperature is needed on one side of the leg than on the other. To serve this purpose, the resistance was made higher on one side by decreasing the width of the trace. Decreasing the cross section of the copper trace will increase the resistance according to Equation 3.3. The uneven heating then causes one side of the polymer to expand more than the other and the

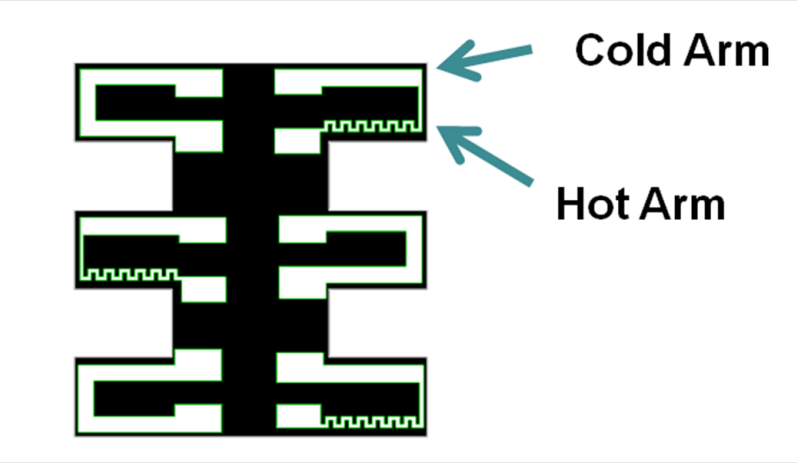

Figure 3.4: The design of the actuators for the walking hexapod microrobot. It will use an alternating tripod gait.

leg experiences a motion similar to MEMS heatuators [26, 27]. However, because this is a bimorph, the leg should experience a twisting motion instead of a sideways bend.

Using the twisting legs in one tripod of the gait as seen in Figure 3.4, and bending actuators for simple lifting legs in the other, a walking robot could be demonstrated. Firstly, the twisting legs would actuate, pushing the robot forward. Then, the alternate legs would actuate, lifting the robot off of the ground. At this point, the robot disengages the twisting actuators, allowing them to reset. Finally, the alternate legs would disengage and the cycle begins again. The alternating actuation result would be comparable to a rowing motion, pushing the robot forward. Repetition of these steps will result in a robot walking forward. A schematic of the proposed walking concept can be seen in Figure 3.5. This would be a crawling robot that could fit within a cubic centimeter and be fabricated in a few hours.

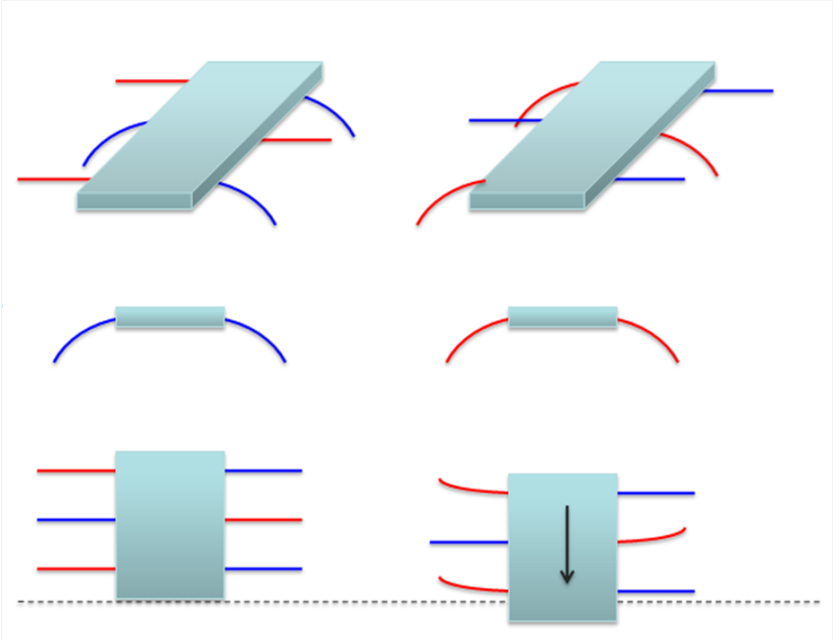

Figure 3.5: The walking concept for the polymer hexapod

3.3.2 *Simulation*

The proposed actuator design using simple uneven traces was simulated in ANSYS ®. Simulation is used here because the analytical solution is expected to be very intensive. This showed that the concept will indeed cause the twisting we expect, but the magnitude of the twisting is small (Figure 3.6). The difference in deflection between the two sides was 100 μm. This validates the concept, however, shows that different designs should be pursued to increase the expected twisting. Higher twisting will result in a larger robot step size.

As a result of the small twisting, a number of new designs directed at improving these twisting results were simulated. One design considered was a serpentine design for the thinner trace as seen in Figure 3.7. This design increases the resistance by increasing the length, and also covers more surface of the polymer to facilitate

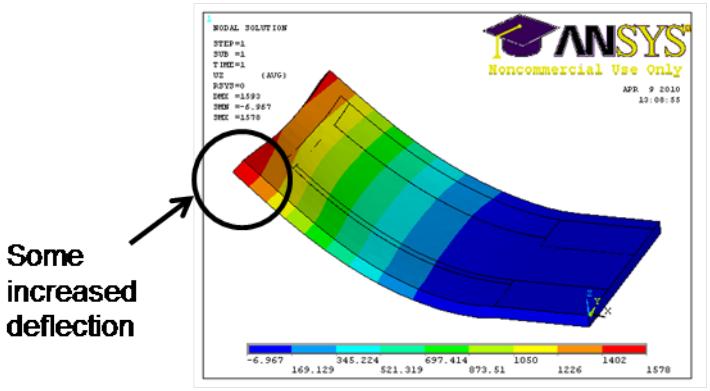

Figure 3.6: Simulation of twisting actuator with uneven metal traces

better and more even heating over the entire side. However, this design was proven unsuccessful because the serpentine shape was able to stretch, similar to a spring, causing the bimorph to not experience the bending desired. An additional design concept tested used the uneven traces as shown before, but with a gap in the polymer layer in the center of the leg. This design would stop the transfer of heat across the leg, creating a higher temperature gradient and thus better twisting. This was simulated and did result in better twisting. The difference in deflection between the two sides was improved to 250μm (Figure 3.8). All simulations discussed here were done with polymer thicknesses of 150 μm.

This simulation does not fully account for all conditions and losses, and assumptions regarding the temperatures were made. For example, these simulations were done assuming a temperature gradient of 85 °C across the leg. This does not account for uneven heating or convection around the edges of the structure. For this reason, these simulations only provide a relative comparison between designs. From these simulations, it can be seen that using a method to block the transfer of

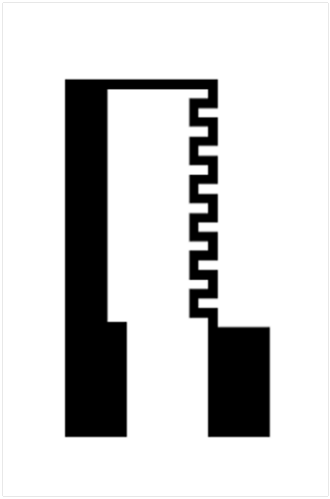

Figure 3.7: The design of serpentine twisting actuators. This design was for the legs that will be used for propelling the microrobot forward, however, simulations showed that this was not the most effective design for twisting

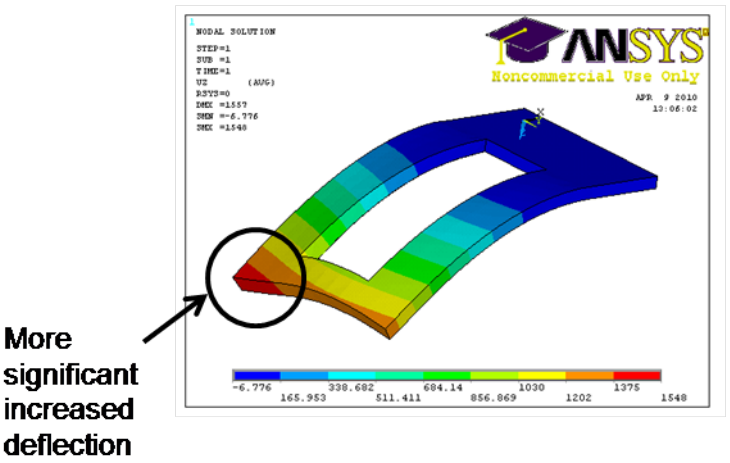

Figure 3.8: Simulation of twisting actuator with uneven traces and gap included in the polymer

heat across the leg, like an air gap in the polymer, is a good way to improve twisting and should be included in future design iterations. As a result, the next step was to develop the process to fabricate these microrobots.

3.4 Fabrication with Integrated Thermal Actuators

3.4.1 *Polymer Process for Hexapod Platform*

A modified version of the RaMP Process described in [28] was used to fabricate the polymer body of the hexapod. In this case, only a Loctite® 3525 is used. As noted in the previous chapter, this product does not have adverse health effects, so no additional protection or equipment is necessary and this section of the fabrication takes place outside of a cleanroom [29].

In the first step, Loctite® 3525 in liquid form is deposited and flattened onto a transparency substrate. Desired thickness of the polymer is achieved by the use of spacers of known thickness such as glass slides or coverslips. For the purpose of this research, a polymer thickness of 150 and 300 μm were used. Because the process requires that the newly formed polymer structures remain on the transparency for later fabrication steps, it was found easiest to put down a transparency layer and then the mask on top of that instead of bringing the polymer directly in contact with the mask. Because the polymer body consists of large feature sizes, the loss in resolution experienced by putting this additional transparency layer between the mask and the polymer does not significantly effect the shape of the hexapod.

The polymer is cured directly under the UV lamp for 27 seconds. At the end of

this time, the mask is removed and the top transparency layer is pulled back slowly. The newly crosslinked polymer structures will stick to this top transparency which serves as a handling layer for the small robots. It is then washed with acetone and the planar hexapod structures remain. Again, all parts of this process were carried out under normal lighting conditions. This process currently only uses one polymer type, but this could be expanded to two or more as was done in the macro-scale case described in Chapter II.

3.4.2 *Actuator Fabrication on Polymer*

Fabrication of the actuators is also a relatively quick and simple process (Figure 3.9). The transparency with the polymer structures is taped to a wafer to give it rigid support for processing. 1 μm of copper is evaporated over the entire surface of the polymer structure using an Temescal®Electron Beam Evaporator. Copper was chosen for its thermal properties as well as its low cost compared with other options like gold. Photoresist is then spun and patterned on the metal coated structures. A bake step was not included. Because the leg features are relatively large in comparison to other micron-scale devices, the large step height that the resist has to be spun over does not pose any significant threat to the integrity of the design. After the resist is patterned, the transparency is removed from the wafer. Then, a diluted 10:1 nitric acid etch is used to etch the exposed copper for an etch time of 4.5 minutes. The possibility of patterning the resist first, then depositing the metal, and subsequently removing the resist to obtain the desired copper designs

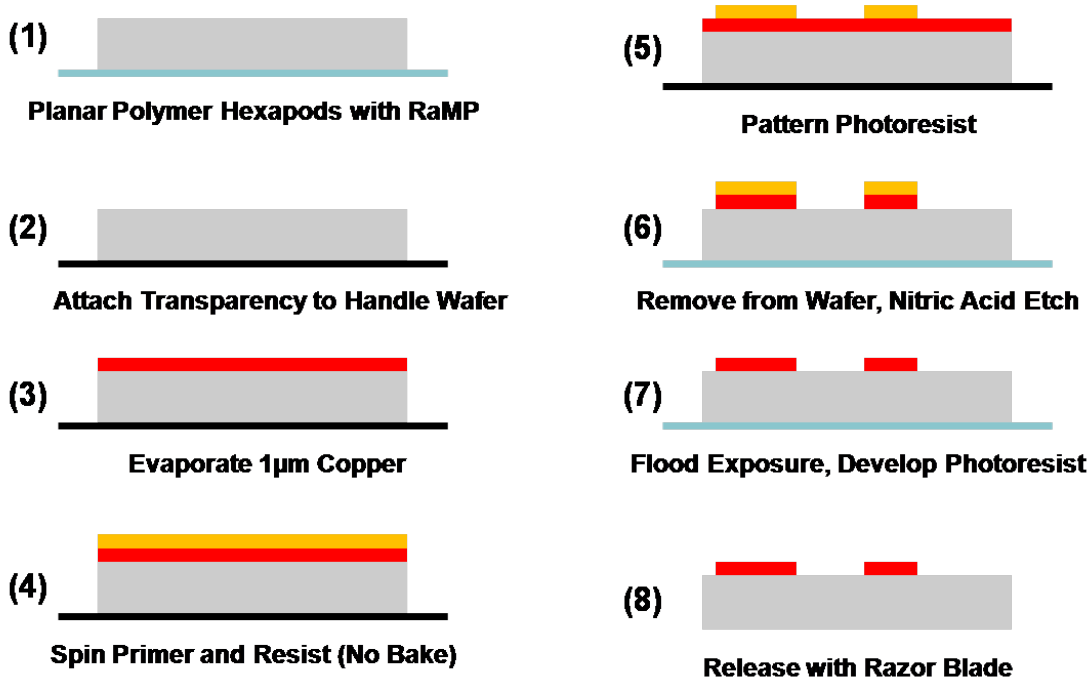

Figure 3.9: The process flow for patterning copper onto polymer hexapods.

was also explored. However, this did not yield good results, and the metal was lifted off the polymer.

To remove the photoresist masking layer, we used a full exposure of the device in UV light with no mask and a second development step. This method was chosen over a typical acetone photoresist removal because it was discovered that the use of acetone on the devices to remove the resist causes a wrinkling and cracking of the metal, significantly increasing the resistance and sometimes breaking the circuit completely. To remove the hexapods and thermal actuators, a razor blade was used to separate the materials. Although the bond is not very strong between the polymer and transparency, care must be taken in this step to avoid cracking the metal traces now on the flexible polymer (Figure 3.10).

Figure 3.10: Cracking of the copper due to over bending of the robot during release from the transparency substrate.

3.5 Robot Results and Demonstrations

3.5.1 *Testing*

After fabricating several devices, testing was conducted to see how close the actual performance of the devices would be to the expected values. The fabrication resulted in a released hexapod with actuated legs. This process from start to finish takes less than a day. The final robot weighs only 30 mg (Figure 3.11).

3.5.2 *Testing of Bimorphs*

Based on calculations of resistance using Equation 3.3 and the resistivity of copper (1.7×10^{-6}ohm-cm), the expected resistance across the bimorph actuators was 0.28 ohms. Experimentally, it was found that the actual resistance was close to 0.9 ohms. This discrepancy is due to mild cracking that occurs in the copper.

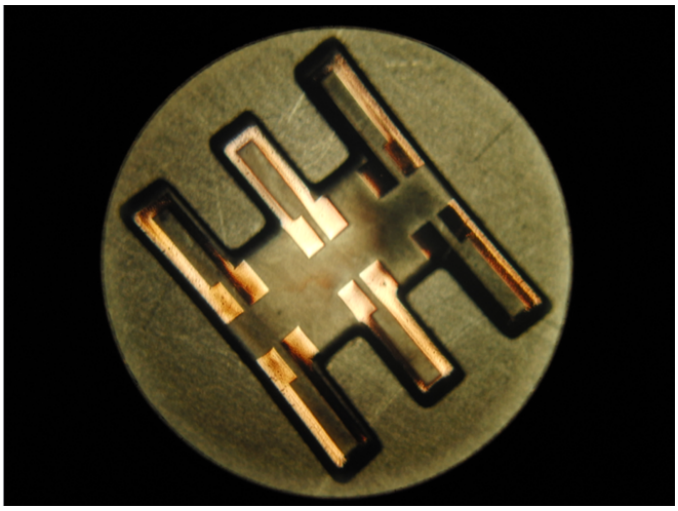

Figure 3.11: Top down view of released planar microrobot platform with patterned copper bending actuators. No control or wiring is shown.

From the calculations in Section 3.2.1, a deformation of 1.58 mm was expected for legs with the 150 μm thick polymer layer. However, observed deflections were on the order of 400 μm as shown in Figure 3.12. This measurement was taken by examination of a video of the deflection. The loss here is expected to be caused by uneven heating of the polymer layer. Although there is significant loss, this deflection is sufficient for lifting the body of the platform off of the ground and a first step towards demonstrating crawling. This demonstration of the actuator on a photo-patternable polymer experimentally validated the bimorph concept.

3.5.3 *Testing of Twisting Actuators*

Twisting actuators were also fabricated and tested to determine the accuracy of the simulation data in Section 3.3.2. The leg was actuated with a current of 200 mA. At this current, it experienced a similar degree of twisting as shown in the

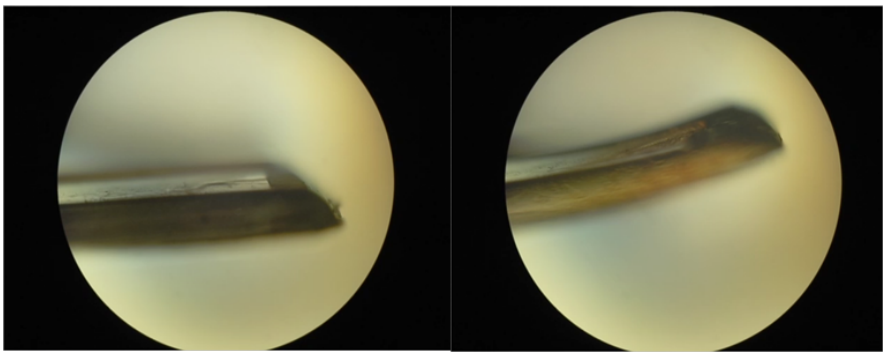

Figure 3.12: Cross-sectional view of the deflection of a 150μm thick leg. The total deflection is about 400 μm, which is enough to lift the body of the hexapod off the surface

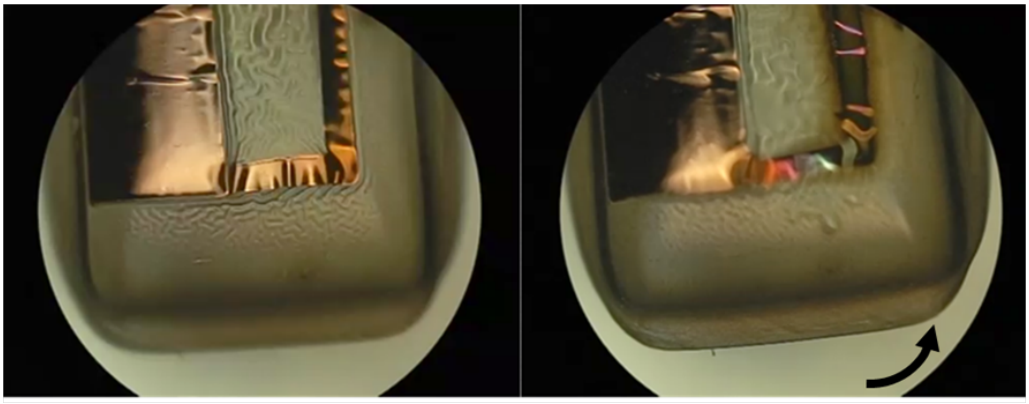

Figure 3.13: Twisting of a leg with uneven traces. The twist was not significant enough to conclude that this design could give the necessary temperature gradient needed across the width of the leg to propel the robot forward.

simulation, approximately 100μm difference in deflection of the sides. This data is taken from inspection. Although this slight twisting did occur, the actuator did not yield the results necessary to cause any significant forward motion (Figure 3.13). This is why more efficient twisting actuators have been designed. Twisting actuators with gaps have yet to be fabricated, but based on the simulations, a much higher degree of twisting is expected from these actuators.

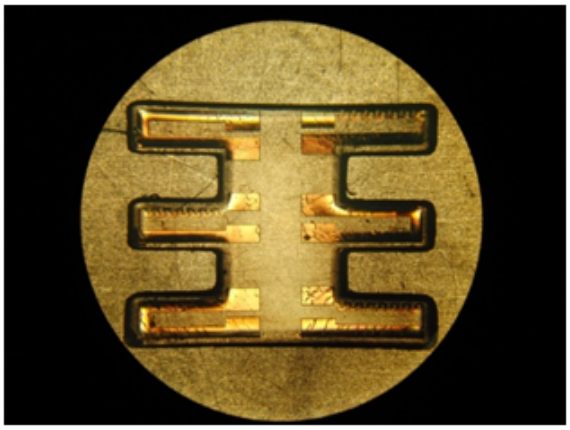

Figure 3.14: A fabricated microrobot with twisting actuators on one tripod of legs.

3.6 Control

The proposed robotic leg is attractive for its ease of fabrication and robustness, but also for its simple control. Because rotation is achieved through the twisting actuators instead of multiple actuators, the leg only requires circuits to control one degree of freedom. The necessary control is therefore simple and lightweight. In addition, for forward walking, only a single signal is required to control each tripod. Therefore, the task of controlling these actuators simplifies to generating two signals to distribute the appropriate amount of current into each set of legs.

A planar microrobot with twisting actuators is shown in Figure 3.14. The control is in four steps as described earlier in Section 3.3.1. This can easily be achieved with a commercial microprocessor and a power stage that could fit on the back of the robot.

The blocked force calculation was done to determine the constraints on power and control and whether this design is feasible for an autonomous, untethered microrobot, which would be the first of its kind to the best knowledge of the authors.

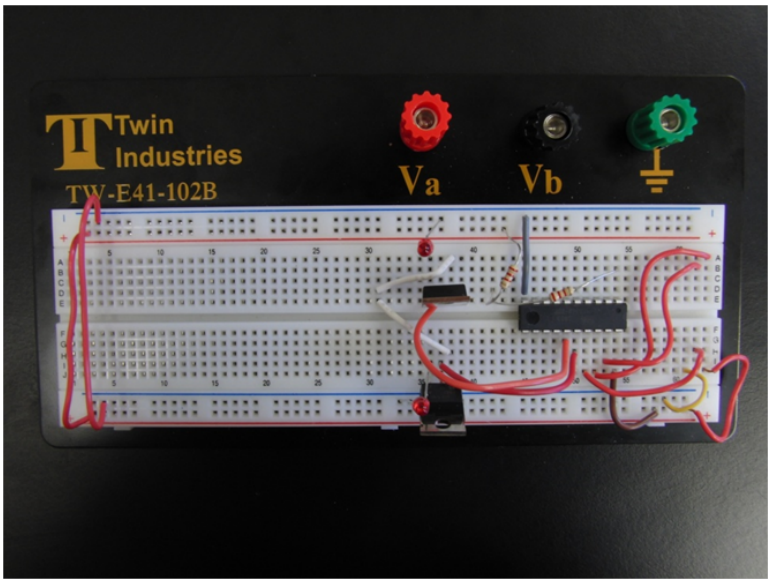

Figure 3.15: A large scale, off-board version of the proposed control.

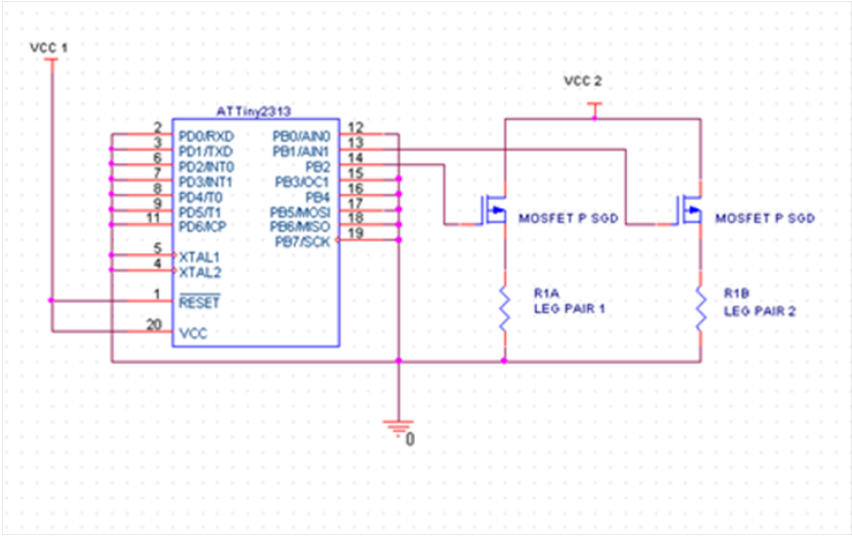

Figure 3.16: The wire diagram for the proposed control scheme.

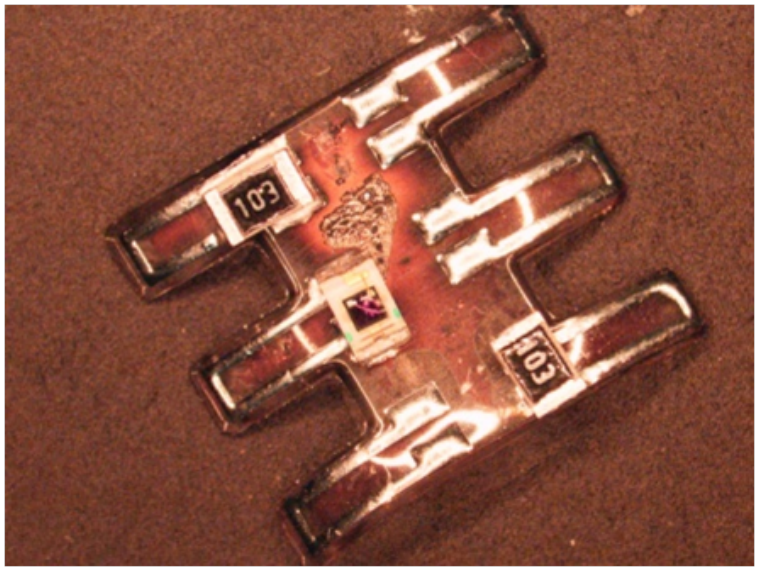

Figure 3.17: Resisters are attached to the copper patterns with a low-temperature solder. Photo Courtesy of Wayne Churaman

Assuming we have three 150 μm legs on the ground that will be used to lift its weight, we have a capacity of a 24.7 gram payload based on the force calculations described earlier in Section 3.2.2. Although a safety of factor should be included due to the assumptions made in the calculations, including full metal cover and even heating, the robot itself weighs only 30 mg. As a result, we should have sufficient force to lift on board control. It is also important to note that this is the blocked force and that it will be less as displacement is added.

A possible on board control scheme was designed. A large scale version of this is shown in Figure 3.15, and a diagram of the circuit is shown in Figure 3.16. This control scheme is very simple. It is comprised of only a microcontroller, ATtiny2313, selected for its small size, and a few MOSFETS to act as switches. The microcontroller can be purchased in a 4mm*4mm package, and the MOSFETS can be even smaller. With commercial products, this circuit can be easily shrunken down to fit

onto the back of the hexapod.

Control integration will be achieved using a low temperature solder. This can be seen in Figure 3.17. Here the low temperature solder coats the metal that is patterned onto the polymer. Then, while still warm, electronic components can be placed on top. This results in an electrical connection upon cooling. Using this process, a chip could be connected to the metal, and eventually, the circuit could be directly written to the polymer. However, this thesis does not cover this work.

3.7 Conclusions and Possible Extensions

With the combination of more efficient twisting actuators and the control described in Section 3.6, a completed walking robot can be realized (Figure 3.18). This design shows the concept and feasibility of fabricating a functional microrobot. The process allows it to be rapidly prototyped and inexpensive. In addition to the ease of fabrication, this leg allows for a very simple control scheme as well as robustness. We have shown the design, analysis, and initial demonstrations as a proof of concept for integrating the platform and actuator to create a thermally actuated walking polymer microrobot with onboard control.

Future research will be optimize the design of the twisting actuators and fabricate them to demonstrate a fully functional walking microrobot. The control will also be optimized and built. The ability to pattern metal directly on the surface of this polymer has also opened up the possibility of pattering the control chip directly on the back of the hexapod. In addition, ideas will be explored to lower the power

Figure 3.18: A mock-up of the final goal of this work.

consumption of the legs to make on-board power more reasonable.

Chapter 4

Applications of Polymer Process

In addition to fabricating the crawling robots that were explored in the previous chapters, there are several other applications of the RaMP process. Working collaboratively with the Army Research Laboratory, the RaMP process has been used to fabricate a polymer hexapod as a skeleton for an untethered jumping microrobot. In addition, this process has been used to fabricate model gills of a Mayfly for fluid dynamic testing. Finally, the RaMP process is also a potential in-house alternative to creating flex PCBs. These will each be described more fully in the coming chapter.

4.1 Jumping Results

Obstacles appear increasingly large to a robot as it shrinks from the macroscale to the micro-scale. The height of these obstacles significantly limits the mobility of crawling robots at this scale. Although flying would circumvent this issue, the power requirements for continuous flight in cm-scale robots are high [2]. Due to these limitations, jumping may be the most effective means of locomotion at the microscale. Researchers at the Army Research Laboratory have made significant progress with research on nanoporous silicon as a propellant [30]. Due to its extremely high power density, it is ideal as a method of providing thrust. However,

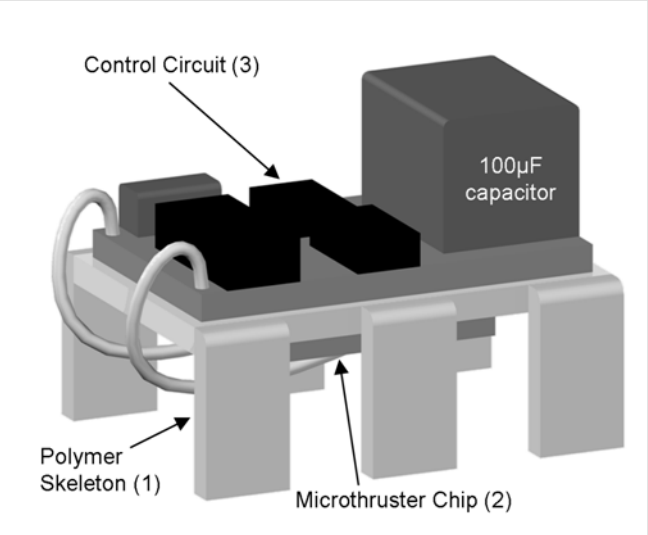

Figure 4.1: Computer model of the jumping microrobot with (1) a polymer skeleton made with the polymer process and (2) nanoporous silicon thruster and (3) control.

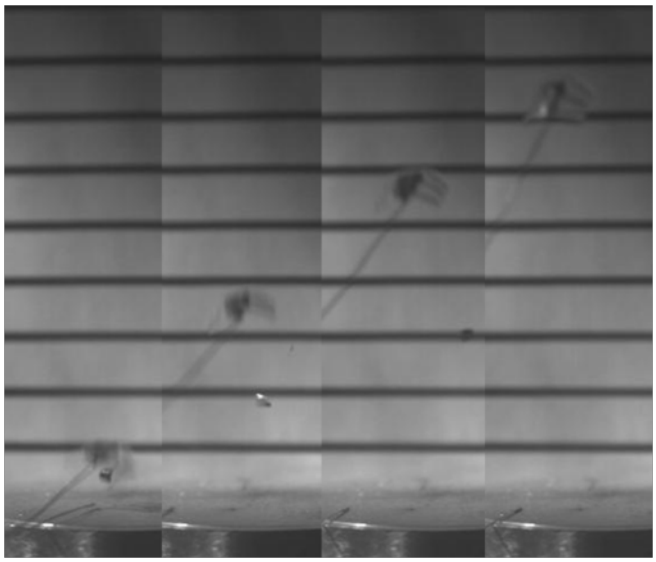

Figure 4.2: Images from a high speed video of a tethered jump. The max height reached was 10cm.

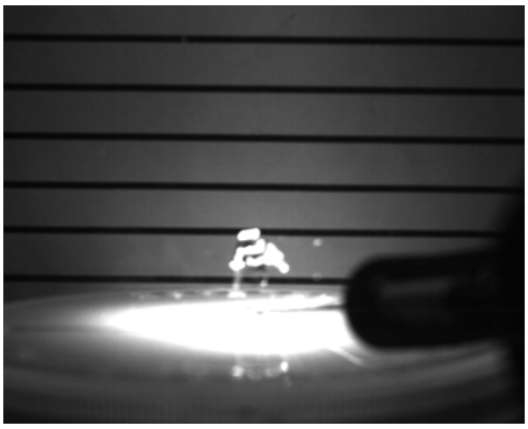

Figure 4.3: Image of an untethered jump of the microrobot. The max height was 1cm.

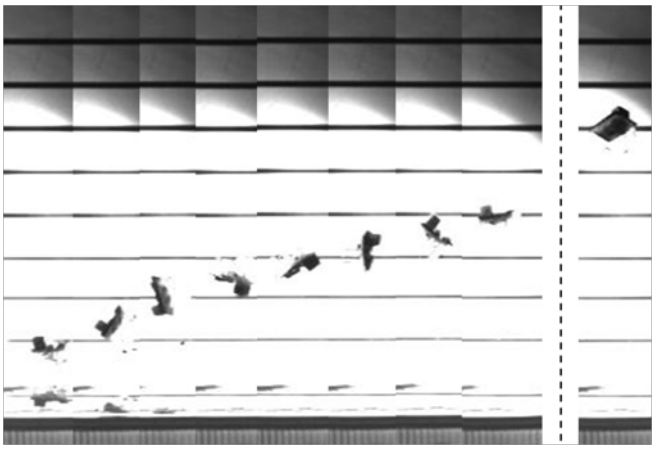

Figure 4.4: Image of a second untethered jump of the microrobot. The max height attained in this jump was 6cm.

to use these actuators in a jumping microrobot, they need to be integrated with electronics. The RaMP process provides a method of packaging all of these items together into the first autonomous jumping microrobot [31].

The platform needed to be robust enough to withstand the ignition of the energetic material as well as the landing. Also, for testing purposes, it needs to be inexpensive and rapidly fabricated. The RaMP Process was used to create this platform. A computer model of the jumping robot concept can be seen in Figure 4.1. A tethered jump of the polymer robot using the nanoporous silicon as actuation was demonstrated. The maximum tethered height achieved was 10cm (Figure 4.2). In addition, two untethered jumps of the microrobot using a platform fabricated with the polymer process were demonstrated. Images of these jumps can be seen in Figures 4.3 and 4.4. Here, the control was put on a chip on the polymer structure. The process was able to rapidly provide a cheap, lightweight, and durable platform to mount electronics and energetic material on to facilitate this jump.

4.2 Mayfly Nymph Gills

The previous section used the RaMP process for packaging parts of microrobot, this section allows for a fast, planar mechanism design. As part of Professor Kenneth Kiger's lab at the University of Maryland, graduate student Mary Larson has been studying the fluid dynamics around the gills of a Mayfly Nymph (Figure 4.5). For testing purposes, they needed to fabricate a gill in which they could embed connections to their test setup. In addition, they wanted to test many shapes and

Figure 4.5: Image of a Mayfly Nymph. Researchers at the University of Maryland are interested in studying the locomotion of these insects (Photo by Mike Higgins. Part of NABS Macroinvertebrates slide collection)

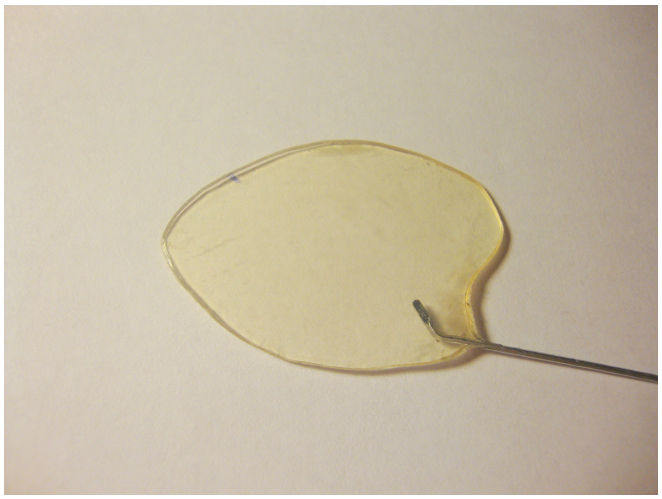

Figure 4.6: Mayfly gill made in the Rapid Microrobot Prototyping Process. Photo courtesy of Mary Larson.

sizes to get the most accurate imitation of the real gills, so being able to be able to change designs easily and quickly was also important. As a result, these gills were made with the polymer process. A completed gill is shown in Figure 4.6. In addition, using this process allowed researchers to premix the polymer with rhodamine before curing. When cured, the polymer-rhodamine mix was fluorescent, allowing them to see it better while testing in a fluid.

4.3 Flexible Circuit Boards

Using the RaMP process to quickly pattern metal directly onto the polymer, flexible circuit boards of a desired shape can be rapidly fabricated. Flexible electronics currently have many applications, but also become very useful in microrobotics and other small electronics where space constraints are a consideration. This is currently being integrated with the jumping robot from the Army Research Laboratory discussed earlier. By patterning the traces directly onto the polymer, the circuit board and the mass and volume it occupies are eliminated. As a result, this will eliminate the weight that the board adds to the robot; a lighter robot will jump higher.

Chapter 5

Conclusions and Contribution

The RaMP Process presented in this thesis is a significant step towards realizing practical robots on this scale. Most of the work can be completed without the use of cleanroom facilities or expensive equipment. The use of Loctite® photo-patternable polymers can create several possibilities in the field of small robotics by eliminating the expense, fragility and complexity of traditional small-scale robots. In this thesis, many new contributions have been made, including a macro-scale low cost and robust process, a micro-scale rapid process, designs for twisting actuators, and process applications to jumping robots, fluid dynamics, and flexible circuits.

A future objective is a fully autonomous walking robot that fits within a cubic centimeter. It has been demonstrated that this process is attractive for prototyping and that, with it, more complex and efficient robots can be realized. Extensions of this work could include integrating more efficient actuators as well as exploring other methods of locomotion to improve robot efficiency. This work will be a building block to demonstrating robots at this size scale. This process is versatile and adaptive, giving it many possible applications in microrobotics as well as in other fields.

Bibliography

[1] A. Hoover, E. Steltz, and R. Fearing, "RoACH: an autonomous 2.4g crawling hexapod robot," Nice, France, Sept. 2008.

[2] S. Bergbreiter and K. S. J. Pister, "Design of an autonomous jumping micro-robot," *IEEE International Conference on Robotics and Automation*, p. 447453, 2007.

[3] J. G. Cham, S. A. Bailey, J. E. Clark, R. J. Full, and M. R. Cutkosky, "Fast and robust: Hexapedal robots via shape deposition manufacturing," *International Journal of Robotics Research*, vol. 21, no. 10-11, pp. 869–882, 2002.

[4] S. Hollar, A. M. Flynn, C. Bellew, and K. S. J. Pister, "Solar powered 10 mg silicon robot," 2003, pp. 706–711.

[5] R. J. Wood, "The first takeoff of a biologically inspired At-Scale robotic insect," *IEEE Transactions on Robotics*, vol. 24, no. 2, pp. 341–347, Apr. 2008.

[6] T. Ebefors, J. U. Mattsson, E. Kalvesten, and G. Stemme, "A walking silicon MicroRobot," Sendai, Japan, 1999, p. 12021205.

[7] B. R. Donald, C. G. Levey, C. D. McGray, I. Paprotny, and D. Rus, "An untethered, electrostatic, globally controllable MEMS MicroRobot," *Journal of Microelectromechanical Systems*, vol. 15, no. 1, pp. 1–15, 2006.

[8] S. Bergbreiter, "Effective and efficient locomotion for Millimeter-Sized microrobots," *IEEE/RSJ International Conference on Intelligent Robots and Systems*, p. 40304035, 2008.

[9] A. M. Dollar and R. D. Howe, "Simple, robust autonomous grasping in unstructured environments," Rome, Apr. 2007, pp. 4693–4700.

[10] J. G. Cham, S. A. Bailey, and M. R. Cutkosky, "Robust dynamic locomotion through feedforward-preflex interaction," Nov. 2000.

[11] N. Tien, "Silicon micromachined thermal sensors and actuators," *Microscale Thermophysical Engineering*, vol. 1, pp. 275–292, 1997.

[12] M. Kohl, *Shape Memory Microactuators*. New York: Springer, 2004.

[13] Y. Bellouard, "Shape memory alloys for microsystems: A review from a material research perspective," *Materials Science and Engineering*, vol. 481-482, pp. 582–589, 2008.

[14] "Loctite, technical data sheet, product 3525," 3525. [Online]. Available: http://www.loctite.tv/template/ying/pdf/docs/3525-EN.pdf

[15] "Loctite, technical data sheet, product 5084," 5084. [Online]. Available: http://www.loctite.tv/template/ying/pdf/docs/5084-EN.PDF

[16] R. Delille, M. G. Urdaneta, S. J. Moseley, and E. Smela, "Benchtop polymer MEMS," *Journal of Microelectromechanical Systems*, vol. 15, no. 5, pp. 1108–1120, Oct. 2006.

[17] R. Sahai, P. Castrataro, and P. Dario, "Adding millimeter-sized, rapidly prototyped robotic structures to microfluidic Lab-on-a-Chip devices," Kobe,Japan, 2009.

[18] M. Schuettler, S. Stiess, B. V. King, and G. J. Suaning, "Fabrication of implantable microelectrode arrays by laser cutting of silicone rubber and platinum foil," *J. Neural Eng.*, vol. 2, 2005.

[19] Q. Chang-jun, M. Pei-sun, and Y. Qin, "A prototype Micro-Wheeled-Robot using SMA actuator," *Sensors and Actuators A*, vol. 113, pp. 93–99, 2004.

[20] R. Yeh, S. Hollar, and K. S. J. Pister, "Single mask, large force, and large displacement electrostatic linear inchworm motors," *Journal of Microelectromechanical Systems*, vol. 11, p. 330336, 2002.

[21] R. Wood, E. Steltz, and R. Fearing, "Optimal energy density piezoelectric bending actuators," *Sensors and Actuators A: Physical*, vol. 119, pp. 476–488, 2005.

[22] P. Potapov and E. D. Silva, "Response time of shape memory alloy actuators," *Journal of intelligent material systems and structures*, vol. 11, no. 125, 2000.

[23] S. Timoshenko, "Analysis of bi-metal thermostats," *Journal of Opt. Soc. Am.*, vol. 11, pp. 233–256, 1925.

[24] N. Lobontiu and E. Garcia, *Mechanics of Microelectromechanical Systems*. Kluwer Academic Publishers, 2005.

[25] R. Sahai, S. Avadhanula, R. Groff, E. Steltz, R. Wood, and R. Fearing, "Towards a 3g crawling robot through the integration of microrobot technologies," 2006.

[26] H. Guckel, J. Klien, T. Christenson, K. Skrobis, M. Laudon, and Lovell, "Thermo-magnetic metal flexure actuators," Hilton Head Island, SC, June 1992, pp. 73–75.

[27] J. Comtois and V. M. Bright, "Surface micromachined polysilicon thermal actuator arrays and applications," Hilton Head Island, SC, June 1996, pp. 174–177.

[28] J. Rajkowski, A. Gerratt, E. Schaler, and S. Bergbreiter, "A Multi-Material millirobot prototyping process," St. Louis, Oct. 2009.

[29] "Loctite 3525 material safety data sheet."

[30] L. Currano, W. Churaman, and C. Becker, "Nanoporous silicon as a bulk energetic material," Denver CO, June 2009, pp. 2172–2175.

[31] L. Currano, W. Churaman, J. Rajkowski, C. Morris, and S. Bergbreiter, "Nanoenergetic silicon as a thrust actuator for jumping microrobots," in *Hilton Head*, June 2010.